

## 2.2 Fully Electronic CMOS DNA Detection Array Based on Capacitance Measurement with On-Chip Analog-to-Digital Conversion

Claudio Stagni Degli Esposti<sup>1</sup>, Carlotta Guiducci<sup>1</sup>, Christian Paulus<sup>2</sup>, Meinrad Schienle<sup>2</sup>, Marcin Augustyniak<sup>3</sup>, Giampaolo Zuccheri<sup>1</sup>, Bruno Samori<sup>1</sup>, Luca Benini<sup>1</sup>, Bruno Riccò<sup>1</sup>, Roland Thewes<sup>3</sup>

<sup>1</sup>University of Bologna, Bologna, Italy

<sup>2</sup>Siemens, Munich, Germany

<sup>3</sup>Infineon Technologies, Munich, Germany

Protein and DNA microarray chips enable the highly parallel investigation concerning the presence and amount of specific proteins or DNA sequences within a given sample. For this purpose, known probe molecules are immobilized on the chip surface, and binding events with matching target molecules from the sample are detected. Today, optical detection techniques are widespread (Fig. 2.2.1, top). There, the target molecules are labeled with fluorescence markers. After the binding and a subsequent washing phase the chip is illuminated, and a fluorescence light image of the array reveals the positions with matching (i.e. chemically bound) probe and target molecules [1].

In Fig. 2.2.1 (bottom), a fully electronic, label-free method is schematically depicted which circumvents expensive optical setups and lowers the biochemical complexity by avoiding the labeling step. The equivalent electrical impedance (modeled by  $R_{sens}$ ,  $C_{sens}$ ) is dominated by the reactive component  $C_{sens}$  because  $R_{sens}$  is very large (due to the quasi-ideal insulating properties of the electrode-solution interface [2]). Chemical binding events close to the surface of the sensor array electrodes lead to a sizable decrease of  $C_{sens}$  [3].

In this work, we present a 16x8 CMOS sensor array for detecting DNA hybridization based on capacitance measurements. A single sensor consists of two interdigitated gold electrodes. The electrode width and spacing are 1µm, the total sensor diameter is 200µm, and the sensor pitch is 300µm. Chips with a total area of 25mm<sup>2</sup> are fabricated in a 0.5µm, 5V standard CMOS process extended with extra steps to process the noble metal [5]. A chip micrograph with a blow-up of a single sensor is shown in Fig. 2.2.7.

Figure 2.2.2 shows the capacitance measurement principle of the circuit underneath each sensor site. A constant current source ( $I_{ref}$ ) is used to alternately charge / discharge the two terminals of the sensor. The voltage difference between the two terminals is monitored using a fully differential comparator. When this amplitude exceeds a defined threshold ( $V_{ref}$ ), all switches change their state so that the charged (discharged) sensor terminal is discharged (charged) again, and the threshold voltage changes polarity. As a consequence, approximately triangular voltage waveforms are obtained at the sensor terminals  $V_A$  and  $V_B$ . The resulting frequency  $f$  of positive threshold crossings is measured by counting  $V_{out}$  pulses. The resulting frequency  $f$  as a function of current and amplitude is given by

$$f = \{ C_{sens} \times R_{sens} \times \ln [ 1 / (1 - V_{ref} / (I_{ref} \times R_{sens})) ] \}^{-1}$$

For not too low frequencies (i.e. not too low values of  $I_{ref}$ ) the contribution of  $R_{sens}$  is negligible and after some mathematics the approximation  $C_{sens} = I_{ref} / (2 V_{ref} f)$  is obtained for the interface capacitance. The frequency range used here is 500Hz to 1kHz.

Figure 2.2.3 shows circuit design details. The sensor current  $I_{ref}$  is provided by cascaded n- and p-MOS current sources. The p-MOS source is part of an in-sensor site p-MOS current mirror biased by an n-MOS current source. The n-MOS current sources bias voltages are generated by an n-MOS cascaded current mirror input stage located at the periphery of the array. A fully-differential amplifier is operated as a comparator, whose number of output pulses within an externally settable time interval is counted by an in-sensor-site 22-stage counter [6], so that fully digital signals are available at the output of the sensor site circuit.

Sensing circuit characterization results are exemplified in Fig. 2.2.4, which shows measured frequencies of the approximately triangular voltage waveform as a function of  $I_{ref}$  for four test circuits. Solid lines correspond to pure single capacitances, 1nF and 4.7nF, respectively, dotted lines to capacitances in parallel with ohmic resistances, 1nF with 200kΩ and 4.7nF with 200kΩ, respectively. Two-terminal sensors on the chip have capacitance values of similar magnitude as compared to these test capacitances. The plot shows that the integrated sensors are able to measure reliably capacitances in this range, even in the presence of a non-negligible parallel resistance  $R_{sens}$  (which may be smaller than expected under unfavourable experimental conditions, due to non-ideal conditions of the molecular layer). Inter-site and inter-chip variations are extremely small (standard deviation = 0.3% within a set of 20 test chips).

Characterization of the chip operated as a DNA sensor is detailed next. Figure 2.2.5 shows the average capacitance variation with respect to bare gold electrodes of: (i) electrodes functionalized with 30-mer probes; (ii) functionalized electrodes with specifically bound complementary 25-mer DNA strands; (iii) functionalized electrodes exposed to non-complementary DNA strands. We observe that, on average, functionalization leads to a decrease in capacitance, and that specific DNA binding leads to a further decrease that is significantly larger than that due to non-specific binding.

Satisfactory multiple-electrode DNA-recognition on a single array is demonstrated in Fig. 2.2.6. There, the relative variation of capacitance is depicted of 12 functionalized electrodes before and after hybridization with complementary DNA samples. The horizontal line shows the worst-case (over more than 50 measurements) electrode capacitance variation due to non-specific binding. The variation due to hybridization is clearly distinguishable from the worst-case due to non-specific binding, even if we consider the error bars obtained by repeating several times electrical measurements and rinsing cycles.

### References:

- [1] M. Schena ed., "DNA Microarrays: A Practical Approach," Oxford University Press, p. 209, Oxford, UK, 2000.
- [2] V. Mirsky et al., "Capacitive Monitoring of Protein Immobilization and Antigen-Antibody Reactions on Monomolecular Alkylthiol Films on Gold Electrodes," *Biosensors and Bioelectronics*, p. 977-989, Jan., 1997.
- [3] C. Guiducci et al., "DNA Detection by Integrable Electronics," *Biosensors and Bioelectronics*, p. 781-787, Mar., 2004.
- [4] C. Berggren et al., "A Feasibility Study of S Capacitive Biosensor for Direct Detection of DNA Hybridization," *Electroanalysis*, p. 156-160, May, 1999.
- [5] F. Hofmann et al., "Fully Electronic DNA Detection on a CMOS Chip: Device and Process Issues," *Tech. Dig. IEDM*, p. 488-491, Dec., 2002.
- [6] M. Schienle et al., "A Fully Electronic DNA Sensor with 128 Positions and In-Pixel A/D Conversion," *ISSCC Dig. Tech. Papers*, pp. 220-221, Feb., 2004.

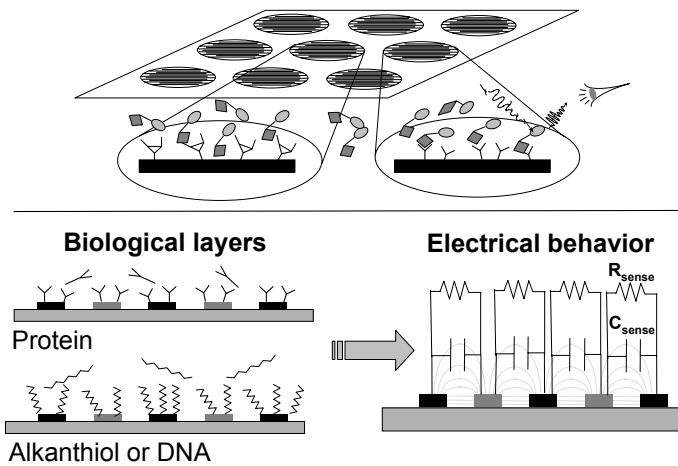


Figure 2.2.1: Schematic description of fluorescence label based operation of micro-arrays and impedance-based label-free fully electronic detection method.

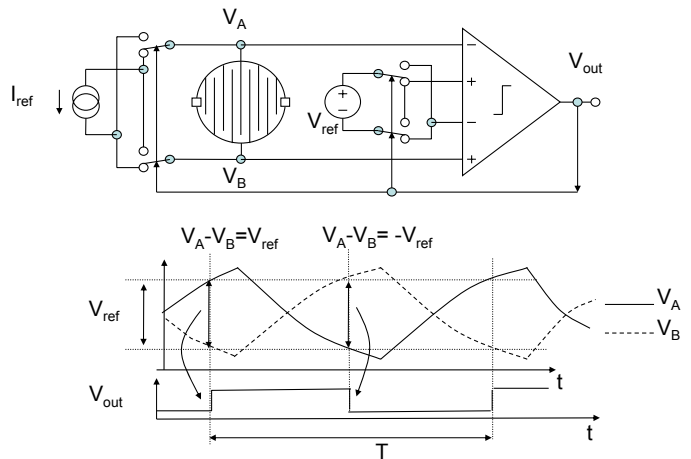


Figure 2.2.2: Detection circuit principle.

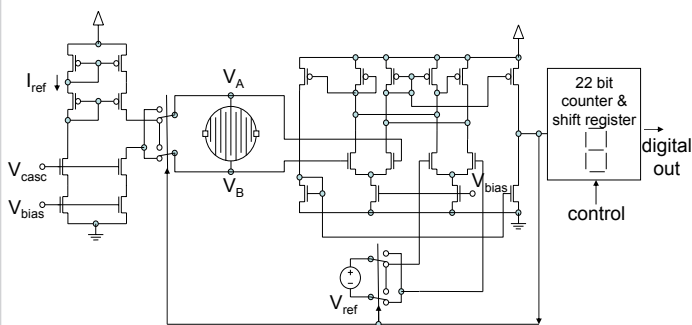


Figure 2.2.3: Diagram of sensor site circuit.

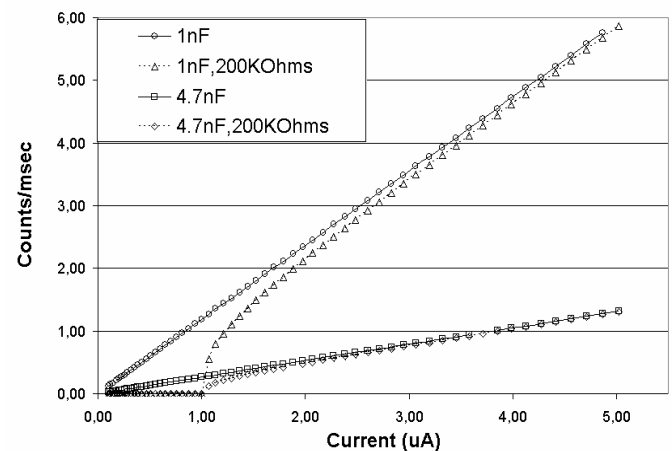


Figure 2.2.4: Measured frequency versus bias current for different test impedances.

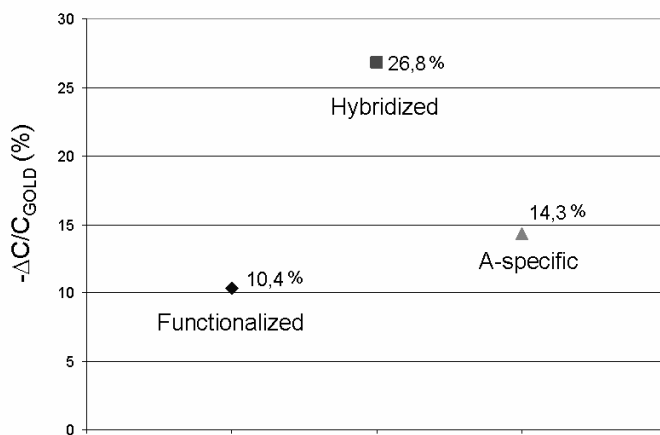


Figure 2.2.5: Capacitance variation (on average) with respect to gold after surface bio-modification.

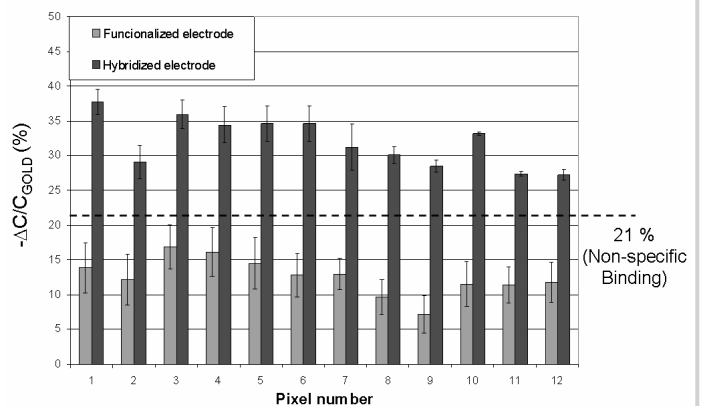


Figure 2.2.6: Multiple sites measurements of DNA hybridization. A reference horizontal line has been added to compare results of hybridized electrodes with the worst-case variation due to non-specific binding.

Continued on Page 636

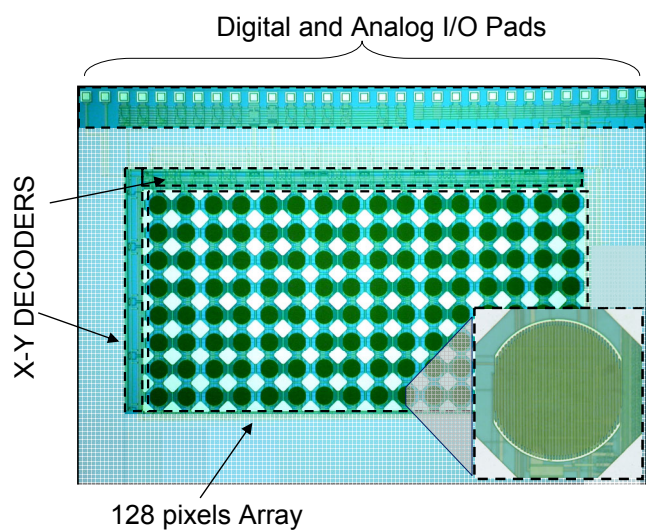


Figure 2.2.7: Chip micrograph. The inset shows a single sensor.